12-13-2017

Effect of counter ions on the self-assembly of polystyrene-polyphosphonium block copolymers

Benjamin Hisey
Western University

Jasmine V. Buddingh
Western University

Elizabeth R. Gillies
Western University, egillie@uwo.ca

Paul J. Ragogna
Western University

Effect of counter ions on the self-assembly of polystyrene-polyphosphonium block copolymers

Benjamin Hisey†; Jasmine V. Buddingh†; Elizabeth R. Gillies†‡; Paul J. Ragogna†*

† Department of Chemistry and Centre for Advanced Materials and Biomaterials Research, The University of Western Ontario, 1151 Richmond Street, London, Canada N6A 5B7
‡ Department of Chemical and Biochemical Engineering, The University of Western Ontario, 1151 Richmond Street, London, Canada N6A 5B9

Abstract

The ability to manipulate block copolymers on the nanoscale has led to many scientific and technological advances. These include nano-scale ordered bulk and thin films and also solution phase components, these are promising materials for making smaller ordered electronics, selective membranes, and also biomedical applications. The ability to manipulate block copolymer material architectures on such small scales has risen from thorough investigations into the properties that affect the architectures. Polyelectrolytes are an important class of polymers that are used to make amphiphilic block copolymers. In this context the authors synthesized polystyrene-*b*-polyphosphonium block copolymers with different anions coordinated to the polyphosphonium block in order to study the effect of the anion on the aqueous self-assembly of the polymers. The anions play an important role in the solubility of the monomeric materials which results in differences in the self-assembly observed through dynamic light scattering and transmission electron microscopy.

Introduction

The self-assembly of amphiphilic block copolymers (BCPs) in solution is a phenomenon that is poised to address a wide range of important technical challenges such as new methods for drug delivery,[1–4] detection and imaging of cancer cells,[5,6] and compartmentalization of reactions.[7–9] Groundbreaking discoveries on the factors that influence the solution phase SA phenomenon have provided the foundations to impact these diverse and highly technical areas. The assembled ordering of amphiphilic BCPs is a balance between the thermodynamic interactions between a copolymer and solvent,[10] the block components in the copolymer (hydrophilic/hydrophobic) and the interactions between individual polymer chains. The importance of the relative lengths of the blocks was well demonstrated in the study by Eisenberg and coworkers, where it was found that even small changes in the relative volume fractions of the blocks of poly(acrylic acid)-*b*-polystyrene (**1**; Figure 1) had significant impacts on the morphological properties of the self-assembled materials.[11] The effects of these interactions have also been observed when self-assembled systems underwent changes in equilibrium structures in response to stimuli such as temperature, pH or the relative amounts of selective and non-selective solvents.[12]

Polyelectrolytes are polymers that contain repeating units with cation/anion pairs. Polyelectrolytes have found a variety of uses as functional components in antimicrobial and antibacterial polymers,[13,14] self-healing polymers,[15] and many other areas.[16] Polyelectrolytes have been used in amphiphilic BCPs as the solvophilic block, thereby promoting solution phase self-assembly. Many groups have studied the self-assembly behavior of amphiphilic polyelectrolyte-*b*-polyneutral copolymers and it has been established that polyelectrolyte blocks in the solution phase self-assembly of copolymers are sensitive to the ionic strength of the

selective solvent because of the imposed solvation states of the corona, as determined by the theoretical work of Borisov and Zhulina.[17] Work by Solomatin and coworkers showed that the stability of nanoparticles formed by complexes of poly(ethylene oxide)-*b*-poly(sodium methacrylate) (**2**; Figure 1) and hexadecyltrimethylammonium bromide was dependent on the identity and concentration of different added salts.[18,19] The effect of added salts on the morphology of nanoparticles formed from polyelectrolyte BCPs was also studied by Förster and coworkers on systems composed of polyethylethylene-*b*-poly(styrenesulfonic acid) (**3**; Figure 1).[20] The authors discovered that by increasing the salt concentration the charged micelles could be induced to fuse into toroidal networks.

More recently, poly(1-(4-vinylbenzyl)-3-methyl imidazolium chloride) (**4** in Figure 1) was subjected to partial ion exchange with hexafluorophosphate to produce a random copolymer of the same backbone repeat unit with randomly associated counterions.[21] These random copolymers then underwent self-assembly due to the differences in the solubilities of the repeat units, depending on the identity of the counter anion. The size of the particles was found to depend on the ratio of the two anions (Cl^- and PF_6^-) associated with the polymer chains. Vijayakrishna and coworkers synthesized a series of BCPs comprising a methacrylate or methacrylamide block and an imidazolium block (**5**; Figure 1). The hydrophilicity of the methacrylate or methacrylamide block could be tuned through the degree of methylation and the hydrophobicity of the imidazolium was altered through anion exchange from a bromide counterion to a bis(trifluoromethane)sulfonimide anion.[22] The *in situ* exchange of the anion led to switching of the location of the block domains in the self-assembled nanostructures as well as alterations in morphological properties.

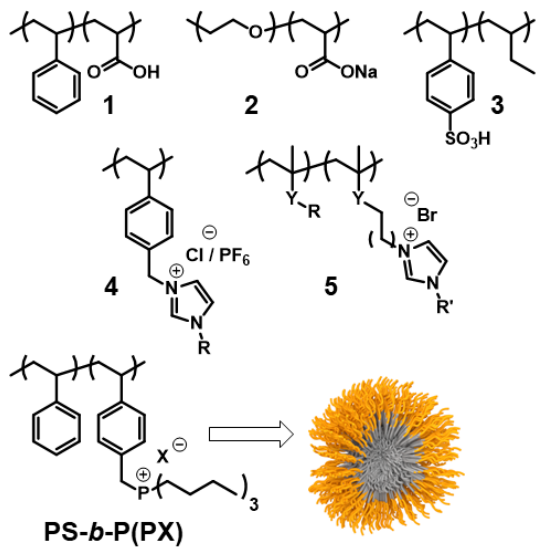

Figure 1. Chemical structures of polyelectrolyte-*b*-polyneutral copolymers (**1** – **5**) that were investigated in previous and those of the current work (**PS-*b*-P(PX)**).

Most amphiphilic BCP systems rely on changing the degree of polymerization of the polymer blocks to affect the morphology of the nano-assemblies. With a hydrophilic block composed of permanently charged phosphonium repeat units, the morphological characteristics of the nano-assemblies can be altered through the presence of different anions. The identity of the counter ion alters the relative hydrophilic volume fraction through the size of the anion itself, as well as the separation of the anion and the cation. Unlike polyneutral solvophilic blocks, in polyelectrolytes the interaction between the same blocks becomes energetically unfavorable because of coulombic repulsion. The repulsion experienced between coronal chains will depend in part on the screening of the coronal charges not only by solvation but by the counter-ions present. While the above work with polymers such as **1** - **5** showed that the identity of the added salt influenced the morphological properties they were unable to ensure that there was only a single counterion present. Furthermore, the addition of salt resulted also in the addition of ions of the same charge as the polymer being studied, which may have also influenced the self-assembled material.

The effect of varying the anion type on the copolymer itself prior to the self-assembly of polyneutral-*block*-polycation into nano scale materials has not been reported to the best of our knowledge. In this context, we have prepared a library of polystyrene-*b*-polyphosphonium (**PS-*b*-P(PX), Figure 1**) copolymers using reversible addition-fragmentation chain transfer (RAFT) polymerization. Each **PS-*b*-P(PX)** system had the same degree of polymerization, but a different counter anion. The effect of the differing cation-anion pairs on the self-assembly was explored. The self-assembly of the polymers was investigated by nano-precipitation of the core forming polystyrene block in the presence of increasing water content from a non-selective solvent. Several morphological characteristics were examined. It was found that the identity of the counter-ion of the **PS-*b*-P(PX)** copolymer did influence the morphological properties of the self-assembled materials. The influence was a result of the differences in anion interaction with the phosphonium block, and differences in the solubility.

Experimental Section

General materials and procedures

Solvents were dried using an MBraun Solvent Purification System. Dried acetonitrile was collected under vacuum in a flame dried Straus flask and stored over 3 Å molecular sieves. Ultrapure water was obtained using a Barnstead EASYPure II ultra pure water system (ThermoFisher Scientific). Tributyl-(4-vinylbenzyl)phosphonium chloride was prepared according to a literature procedure.[23] Nuclear Magnetic Resonance (NMR) spectroscopy was conducted on a Varian INOVA 400 MHz spectrometer (^{1}H 400.09 MHz, $^{31}P\{^{1}H\}$ 161.82 MHz, $^{13}C\{^{1}H\}$ 100.52 MHz) unless otherwise noted. All ^{1}H NMR spectra were referenced relative to $SiMe_4$ (residual solvent in $CDCl_3$; ^{1}H $\delta = 7.27$). The chemical shifts for $^{31}P\{^{1}H\}$ NMR spectroscopy were referenced using an external standard (85% H_3PO_4; $\delta_P = 0$). All $^{13}C\{^{1}H\}$ NMR spectra were referenced relative to $SiMe_4$ (residual solvent in $CDCl_3$; $\delta_C = 77.0$). Infrared spectra were recorded using a Bruker Tensor 27 spectrometer using attenuated total internal reflectance mode (ATR) on a ZnSe crystal. Electrospray Ionisation (ESI) Mass spectrometry was obtained on a Finnigan MAT 8400 mass spectrometer using electron impact ionization. Dynamic Light Scattering (DLS) and ζ-potential measurements were performed on a Zetasizer Nano ZS (Malvern Instruments) using a 633 nm laser. Solutions of approximately 0.1 mg/mL of polymer were used in DLS measurements. Ultraviolet-visible (UV-Vis) spectroscopy was performed using a Varian Cary 300 Bio UV-Visible spectrophotometer. Size exclusion chromatography (SEC) of the MacroRAFT agent was performed on a Viscotek GPC Max VE2001 solvent module (Malvern Instruments Ltd., Malvern, U.K.). Samples were analyzed using the Viscotek VE3580 RI detector operating at 30 °C. The separation technique employed two Agilent Polypore (300 X 7.5 mm) columns connected in series with a Polypore guard column (50 X 7.5

mm; Agilent Technologies). Samples were dissolved in tetrahydrofuran (glass distilled) at a concentration of approximately 5 mg/mL, filtered through 0.22 μm syringe filters, and then injected using a 100 μL loop. The THF eluent was filtered and eluted at 1 mL/min for a total of 30 min. The instrument was calibrated with PS standards. Dispersities (*Đ*) are listed to two decimal places, and the degree of polymerization (DP) for the styrene polymer was determined by SEC. The SEC of the BCPs was performed on a Malvern VISCOTEK GPCmax instrument equipped with a VISCOTEK VE 3580 RI detector and two Inert series columns (P101609 and Q10183) at a constant temperature of 50 °C. The eluent was 0.4 M tetrabutylammonium triflate in DMF with a flow rate of 1 mL/min. Calibration was performed using narrow PMMA standards. TEM images were obtained using a Philips CM 10 Transmission Electron Microscope. Self-assembled samples were loaded onto Formvar coated copper grids by holding the grid with self-closing tweezers, placing a 5.0 μL drop of a 0.5 – 1.0 mg/mL solution onto the grid, and wicking away the excess after 1 min. Dialysis was performed using Spectra/Por® 6 pre-wetted dialysis tubing (Spectrum Laboratories Inc.).

Synthesis of 4-vinylbenzyl bromide, ***6***

To a stirring suspension of anhydrous lithium bromide (6.00 g, 69.1 mmol) in 15 mL of anhydrous THF, 4-vinylbenzyl chloride (6.00 mL, 38.3 mmol) was added in a N_2 filled glovebox. The suspension was stirred overnight at room temperature. The following day the solvent was removed under vacuum and the mixture was suspended in 30 mL dry CH_2Cl_2 and filtered. The filtrate was washed three times with water (20 mL). The organic layer was dried with $MgSO_4$ and the volatiles were removed under vacuum to yield a light-yellow oil. The product was used without further purification (5.80 g, 78% yield); ^{1}H NMR (400 MHz, $CDCl_3$):

δ = 7.37 (m, *Ar*H, 4H); 6.70 (dd, ^{3}J(H,H) = 11.2 Hz, ^{3}J(H,H) = 17.6 Hz, =*C*H, 1H); 5.77 (d, ^{3}J(H,H) = 17.6 Hz, *trans*, 1H); 5.28 (d, ^{3}J(H,H) = 11.2 Hz, *cis*-, 1H); 4.57 (s, *C*H_2 *on 4-vinylbenzyl chloride*); 4.48 (s, *C*H_2, 2H).

Synthesis of tributyl-(4-vinylbenzyl)phosphonium bromide, ***7-Br***

To a stirring solution of 4-vinylbenzyl bromide (2.00 g, 10.1 mmol) in 10 mL of anhydrous CH_3CN in a pressure flask in a N_2 filled glovebox, tributyl phosphine (1.70 g, 8.4 mmol) was added dropwise. The reaction mixture warmed with the addition of the phosphine. The flask was capped and stirred at room temperature. After one hour, the ^{31}P-NMR showed the conversion of the phosphine to a single product. The volatiles were removed under vacuum. The resulting oil was dissolved in minimum CH_2Cl_2 and the product was precipitated out of solution in excess, cold stirring hexanes. The light orange powder was collected by vacuum filtration. (2.83g, 84% yield) ^{1}H NMR (400 MHz, $CDCl_3$): δ = 7.39 (s, Ar*H*, 4H); 6.67 (dd, ^{3}J(H,H) = 17.6 Hz, ^{3}J(H,H) = 11.2 Hz, CH_2=C*H*, 1H); 5.76 (d, ^{3}J(H,H) = 17.6 Hz, *cis*- alkene, 1H); 5.29 (d, ^{3}J(H,H) = 10.8 Hz, *trans*- alkene, 1H); 4.26 (d, ^{3}J(H,P) = 15.2 Hz, PC*H*$_2$C$_q$, 2H); 2.40 (m, PC*H*$_2$, 6H); 1.47 (m, C*H*$_2$, 12H); 0.92 (t, ^{3}J(H,H) = 6.6 Hz, C*H*$_3$, 9H). ^{13}C{^{1}H} (100.52 MHz, $CDCl_3$): δ = 137 (s, 3° alkene, 1C); 135 (d, ^{5}J(C,P) = 2 Hz, 4° aromatic, 1C); 130 (d, ^{3}J(C,P) = 5 Hz, 3° aromatic, 2C); 127 (d, ^{2}J(C,P) = 8.8 Hz, 4° aromatic, 1C); 127 (s, 3° aromatic, 2C); 114 (s, H_2C=, 1C); 27 (d, ^{1}J(C,P) = 45 Hz, CH_2P, 1C); 24 (d, ^{1}J(C,P) = 15 Hz, CH_2P, 3C); 23 (d, ^{2}J(C,P) = 4 Hz, CH_2, 3C); 18 (d, ^{3}J(C,P) = 46 Hz, CH_2, 3C); 13 (s, CH_3, 3C). ^{31}P{^{1}H} NMR (161.82 MHz, $CDCl_3$): δ = 31.8. ATR-IR: 1630 cm^{-1} (w, C=C-H); 2870 cm^{-1} (s, alkane C-H); 2920 cm^{-1} (m, aryl C-H); 2960 cm^{-1} (s, alkenyl C-H).

Synthesis of tributyl-(4-vinylbenzyl)phosphonium nitrate, ***7-NO$_3$***

To a rapidly stirring aqueous solution of tributyl-(4-vinylbenzyl)phosphonium chloride in 4 mL of water (2.00 g, 5.6 mmol) an aqueous solution of silver nitrate in 4 mL of water (1.00 g, 5.8 mmol) was slowly added. A white precipitate formed upon mixing and the solution was stirred for 1 hour. The suspension was filtered and a drop of aqueous silver nitrate solution was added. If a white precipitate formed, the process was repeated until no further precipitate formed.[24] Upon complete reaction of the chloride monomer, the aqueous phase was extracted ten times with 15 mL of CH_2Cl_2. The organic phases were combined, dried with $MgSO_4$, filtered, and the volatiles were removed in vacuo to yield a clear colourless oil which cooled to a waxy solid. (1.87 g, 88% yield). ^{1}H NMR (400 MHz, $CDCl_3$): δ = 7.39 (d, ^{3}J(H,H) = 8.0 Hz, 2H); 7.27 (dd, ^{3}J(H,H) = 8.6 Hz, ^{4}J(H,P) = 3.0 Hz, 2H); 6.68 (dd, ^{3}J(H,H) = 17.6 Hz, ^{3}J(H,H) = 11.2 Hz, CH_2=C*H*, 1H); 5.76 (d, ^{3}J(H,H) = 17.6 Hz, *cis*- alkene, 1H); 5.30 (d, ^{3}J(H,H) = 10.8 Hz, *trans*-alkene, 1H); 3.93 (d, ^{3}J(H,P) = 14.8 Hz, PC*H*$_2$C$_q$, 2H); 2.23 (m, PC*H*$_2$, 6H); 1.45 (m, C*H*$_2$, 12H); 0.92 (t, ^{3}J(H,H) = 6.8 Hz, C*H*$_3$, 9H). ^{13}C{^{1}H} (100.52 MHz, $CDCl_3$): δ = 138 (d, ^{6}J(C,P) = 3.9 Hz, 2° alkene, 1C); 135 (d, ^{5}J(C,P) = 1.9 Hz, 4° aromatic, 1C); 129 (d, ^{3}J(C,P) = 5.0 Hz, 3° aromatic, 2C); 127 (d, ^{2}J(C,P) = 8.8 Hz, 4° aromatic, 1C); 126 (d, ^{4}J(C,P) = 3.3 Hz, 3° aromatic, 2C); 113 (d, ^{7}J(C,P) = 1.5 Hz, 1° alkene, 1C); 25 (d, ^{1}J(C,P) = 45.1 Hz, PCH_2, 1C); 23 (d, ^{1}J(C,P) = 15.7 Hz, PCH_2, 3C); 22 (d, ^{2}J(C,P) = 4.7 Hz, CH_2, 3C); 17 (d, ^{3}J(C,P) = 47.3 Hz, CH_2, 3C); 12 (s, CH_3, 3C). ^{31}P{^{1}H} NMR (161.82 MHz, $CDCl_3$): δ = 31.8. ATR-IR: 1330 cm^{-1} (s, N-O); 1600 cm^{-1} (w, C=C-H); 2870 cm^{-1} (s, alkane C-H); 2935 cm^{-1} (m, aryl C-H); 2955 cm^{-1} (s, alkenyl C-H).

Synthesis of tributyl-(4-vinylbenzyl)phosphonium triflate, ***7-OTf***

To a rapidly stirring solution of tributyl-(4-vinylbenzyl)phosphonium chloride (2.50 g, 7.0 mmol) in CH_2Cl_2, a solution of lithium triflate in CH_2Cl_2 (2.18 g, in 5 mL) was added. A white precipitate formed upon mixing and the solution was stirred overnight. The suspension was filtered and a drop of lithium triflate solution in CH_2Cl_2 was added. If a white precipitate formed the process was repeated until no further precipitate formed. Upon complete reaction of the chloride monomer, the organic phase was washed three times with water (20 mL), dried over $MgSO_4$, filtered, and the volatiles were removed in vacuo. The product was a white powder. (3.03 g, 92% yield). ^{1}H NMR (400 MHz, $CDCl_3$): δ = 7.36 (d, ^{3}J(H,H) = 8.0 Hz, 2H); 7.25 (dd, ^{3}J(H,H) = 8.2 Hz, ^{4}J(H,P) = 2.2 Hz, 2H); 6.66 (dd, ^{3}J(H,H) = 17.8 Hz, ^{3}J(H,H) = 11.0 Hz, CH_2=C*H*, 1H); 5.74 (d, ^{3}J(H,H) = 17.6 Hz, *cis*- alkene, 1H); 5.29 (d, ^{3}J(H,H) = 11.2 Hz, *trans*-alkene, 1H); 3.78 (d, ^{3}J(H,P) = 15.2 Hz, PCH_2C$_q$, 2H); 2.15 (m, PCH_2, 6H); 1.14 (m, CH_2, 12H); 0.90 (m, CH_3, 9H). ^{13}C{^{1}H} (100.52 MHz, $CDCl_3$): δ = 137 (d, ^{6}J(C,P) = 4 Hz, 2° alkene, 1C); 135 (d, ^{5}J(C,P) = 2 Hz, 4° aromatic, 1C); 130 (d, ^{3}J(C,P) = 5 Hz, 3° aromatic, 2C); 127 (d, ^{2}J(C,P) = 9 Hz, 4° aromatic, 1C); 127 (d, ^{4}J(C,P) = 3 Hz, 3° aromatic, 2C); 120 (q, ^{1}J(C,F) = 320 Hz, F_3CSO_3, 1C); 115 (s, H_2C=, 1C); 26 (d, ^{1}J(C,P) = 45 Hz, CH_2P, 1C); 23 (d, ^{1}J(C,P) = 15 Hz, CH_2P, 3C); 23 (d, ^{2}J(C,P) = 5 Hz, CH_2, 3C); 18 (d, ^{3}J(C,P) = 47 Hz, CH_2, 3C); 13 (s, CH_3, 3C). ^{31}P{^{1}H} NMR (161.82 MHz, $CDCl_3$): δ = 32.3. ATR-IR: 635 cm^{-1} (s, S-O); 1030 cm^{-1} (s, S-O); 1160 cm^{-1} (m, CF_3); 1225 cm^{-1} (m, CF_3); 1270 cm^{-1} (s, SO_3); 1625 cm^{-1} (w, C=C-H); 2875 cm^{-1} (s, alkane C-H); 2935 cm^{-1} (m, aryl C-H); 2955 cm^{-1} (s, alkenyl C-H).

Synthesis of the polystyrene macro-RAFT agent

The synthesis of the dodecyl-(4-trifluoromethylbenzyl)trithiocarbonyl RAFT agent followed a previously reported procedure with the following differences.[23] After quenching the reaction, the

reaction mixture was poured into rapidly stirring excess methanol and a light-yellow precipitate formed. The precipitate was collected as a light yellow powder, but contained large amounts of styrene monomer. The polymer was redissolved in CH_2Cl_2 and precipitated in excess stirring methanol. This process was repeated until the complete removal of styrene monomer was achieved as determined by the absence of the monomer signals in the ^{1}H-NMR spectrum of the macro-RAFT agent. The product was a light yellow powder. (9.4 g, 96% yield). ^{1}H NMR (400 MHz, $CDCl_3$): δ = 7.09 (m, 3H, *para*- and *meta*- aryl); 6.50 (m, 2H, *ortho*- aryl); 2.30 – 1.30 (m, 3H, alkyl). DP = 390, $Đ$ = 1.14, M_w = 40,500 g/mol

General synthetic procedure of macro-RAFT polymerization of phosphonium copolymers

The macro-RAFT agent (1.00 g, 25 μmol) and **7-Cl** as an example (110 mg, 308 μmol) were dissolved in (10 mL) of degassed THF (3 x freeze-pump-thaw). Sonication was used to ensure the macro-RAFT agent and monomer were fully dissolved. AIBN (1.4 mg, 8 μmol) was added to the reaction mixture and the solution was purged with N_2 at room temperature for five minutes with stirring. After purging, the flask was placed in an 80 °C oil bath for 20 hours. The flask was removed from the oil bath and placed in liquid nitrogen for one minute. The product was obtained by precipitating the copolymer in isopropanol and unreacted monomer was removed by washing with isopropanol. The product was an off-white powder.

PS$_{390}$*-b-*P(7-Cl)$_7$ (958 mg, 90.4 % yield). ^{1}H NMR (400 MHz, $CDCl_3$): δ = 7.2 – 7.0 (m, aryl - *ortho*- and *para*- to backbone); 6.9 – 6.3 (m, 794H, aryl *meta*- to backbone); 2.43 (m, benzylic, *α* to P); 2.21 (m, methylene *α* to P); 2.18 – 1.30 (m, 1275H, alkyl not otherwise assigned); 0.91 (m, 61H, CH_3). ^{31}P{^{1}H} NMR (161.82 MHz, $CDCl_3$): δ = 31.8. $Đ$ = 1.36, M_n (by SEC) = 31,500 g/mol, M_n (by ^{1}H-NMR) = 37,060 g/mol

PS$_{390}$*-b-*P(7-Br)$_7$ (968 mg, 91.2 % yield). ^{1}H NMR (400 MHz, $CDCl_3$): δ = 7.1 – 6.9 (m, aryl - *ortho*- and *para*- to backbone); 6.8 – 6.2 (m, 794H, aryl *meta*- to backbone); 2.44 (m, methylene *α* to P); 2.2 – 1.3 (m, 1275H, alkyl not otherwise assigned); 0.94 (m, 61H, CH_3). $^{31}P\{^1H\}$ NMR (161.82 MHz, $CDCl_3$): δ = 31.5. M_n (by ^{1}H-NMR) = 37,700 g/mol

PS$_{390}$*-b-*P(7-NO$_3$)$_7$ (852 mg, 86.7 % yield). ^{1}H NMR (400 MHz, $CDCl_3$): δ = 7.2 – 6.9 (m, aryl - *ortho*- and *para*- to backbone); 6.8 – 6.2 (m, 794H, aryl *meta*- to backbone); 2.27 (m, methylene *α* to P); 2.2 – 1.3 (m, 1275H, alkyl not otherwise assigned); 0.92 (m, 61H, CH_3). $^{31}P\{^1H\}$ NMR (161.82 MHz, $CDCl_3$): δ = 31.9. *Đ* = 1.4, M_n (by SEC) = 35,300 g/mol, M_n (by ^{1}H-NMR) = 37,600 g/mol

PS$_{390}$*-b-*P(7-OTf)$_7$ (862 mg, 88.6 % yield). ^{1}H NMR (400 MHz, $CDCl_3$): δ = 7.1 – 6.9 (m, aryl - *ortho*- and *para*- to backbone); 6.8 – 6.2 (m, 794H, aryl *meta*- to backbone); 2.15 (m, methylene *α* to P); 2.1 – 1.3 (m, 1275H, alkyl not otherwise assigned); 0.89 (m, 61H, CH_3). $^{31}P\{^1H\}$ NMR (161.82 MHz, $CDCl_3$): δ = 31.4. ^{19}F NMR (376.50 MHz, $CDCl_3$): δ = -62.5 (s, 3F, RAFT endgroup); -78.4 (s, 21F, triflate). *Đ* = 1.4, M_n (by SEC) = 36,500 g/mol, M_n (by ^{1}H-NMR) = 38,200 g/mol

Kinetically trapped self-assembly of phosphonium BCPs

PS-*b*-P(PX) (2.5 mg) was dissolved in 0.5 mg of DMF or THF as non-selective solvents. For the organic-into-water addition, the BCP solution was quickly added to rapidly stirring ultra-pure water (2.0 mL). For the water-into-organic addition, the ultra-pure water (2.0 mL) was added stirred BCP solution slowly over ten minutes. In the case of THF as the non-selective solvent, the suspension was placed in a 35°C sand bath overnight to evaporate the THF. In the case of DMF as the non-selective solvent, the suspension was transferred to a 10 kg/mol molecular weight cut-off dialysis membrane (Spectra/Por® 6 Standard RC Pre-wetted dialysis tubing, 28 mm flat

width) and dialyzed against 100 mL of ultra-pure water with one replacement of the dialysate over a 14 hour period.

Solvent annealed self-assembly of phosphonium BCPs

PS-*b*-P(PX) (2.5 mg) was dissolved in 0.5 mg of DMF or THF as non-selective solvents. For the organic-into-water addition, the BCP solution was quickly added to rapidly stirring ultra-pure water (2.0 mL). For the water-into-organic addition, the ultra-pure water (2.0 mL) was added to a stirring BCP solution slowly over ten minutes. The resulting suspensions were allowed to anneal at room temperature for 96 hours. 100 μL of the annealed suspension was added into 1900 μL of ultra-pure water to quench the annealing and give a final concentration of 0.5 mg/mL of BCP and a 1% solution of the non-selective solvent.

Determination of critical aggregation concentration

Note that only the fast water addition to THF systems were used. The assemblies were prepared as stated above except approximately 5 mg of copolymer was used. The resulting suspension was diluted by two-fold steps, 10 times. The dilutions were added into vials containing nile red dye, introduced by the evaporation of 100 μL of a 6.03 μM CH_2Cl_2 solution. The nile red solution was prepared by dissolution of 1.92 mg in 10.0 mL of CH_2Cl_2. The vials were agitated overnight on a wrist action shaker and the following day the fluorescence of the diluted suspensions was measured. The fluorescence intensity was plotted against the log of the concentration of the samples and the CAC was taken as the concentration at the point of intersection of the two lines generated from the two regions of slope on the plot.

Determination of K_{ow}

The partition of the **7-X** salts between 1-octanol and ultrapure water was determined spectroscopically with ^{31}P NMR and in triplicate. The 1-octanol was washed three times with a 1M NaOH solution and dried over $MgSO_4$ before use. A ^{31}P NMR standard of Ph_3P was made by dissolving 179 mg of Ph_3P into 5.00 mL of 1-octanol. The **7-Cl** and **7-Br** salts were dissolved in ultra pure water to give a concentration of 10.0 mg/mL. Due to the low water solubility of **7-NO_3** and **7-OTf**, they were dissolved in 1-octanol at a concentration of 10.0 mg/mL. In a centrifuge tube, 1 mL of the stock **7-X** solution was added to 1 mL of the opposing solvent. These were gently stirred on a wrist action shaker at room temperature for 16 hours. The samples were then centrifuged the following morning and 500 μL of the 1-octanol phase was added to 300 μL of the Ph_3P standard solution and 200 μL of 1-octanol. The relative integration of the **7-X** ^{31}P NMR signal to the Ph_3P ^{31}P NMR signal was used to determine the concentration of **7-X** in the octanol phase. The octanol-water partition coefficient (K_{ow}) is determined with the following equation:

$$K_{ow} = \frac{[solute]_{OctOH}}{[solute]_{H2O}}$$

Results and Discussion

Synthesis of Phosphonium Monomers

The morphological properties of the self-assembled materials are dependent on the relative degrees of polymerization (DP) of the two blocks. In a study of the effect of anion identity on self-assembly, it was clear that there were two approaches to accessing polymers with the same DP of the blocks and different anions. The first was to make the polymers with monomers with different anions and the other was to make the polymer and to exchange the anion. The second method presents a challenge in confirming that complete conversion is achieved from one anion to the next, and requires more difficult experimental conditions for achieving the exchange due to the amphiphilicity of the BCP. Therefore, in this work the first method was used, as this allowed the full characterization of the identity of the anion on the monomer as well as the investigation of the anion effect on some of the monomer properties.

Understanding the effect of solution phase cation-anion interactions on polymer SA required some variation in the electronics and lipophilicity of the anionic species, so a series of anions was selected. The halide anions (Cl^-, Br^-) have spherical charge distributions, the difference being that the bromide is much larger, more polarizable, and more lipophilic. Therefore **7-Br** exhibits a lower aqueous solubility than **7-Cl**. While the nitrate salt **7-NO_3** K_{ow} close to 1.00, the ionic radius is similar to that of bromide.[25] The triflate anion was much more lipophilic and thus **7-OTf** has limited aqueous solubility. Taken together, these anions represent different charge densities, sizes and aqueous solubilities, properties that impact the self-assembly of the resultant BCPs.

The chloride and bromide analogues (**7-Cl/Br**) were synthesized via quaternization of tri(n-butyl)phosphine with 4-vinylbenzyl chloride or its bromide analogue **6**, synthesized from

the former via a Finkelstein reaction (Scheme 1). The reaction proceeded to at least 98% conversion in each case, as determined by the relative integrations of the ^{1}H NMR spectra for the methylene protons at 4.57 ppm for 4-vinylbenzyl chloride and 4.48 ppm for 4-vinylbenzyl bromide (Figure S2). The onwards quaternization reaction was carried out without separation of the chloride analogue because of the extremely similar nature of the vinylbenzyl halides. Nevertheless, the formation of **7-Br** was the preferred product because of the enhanced reactivity of **6** (i.e. heavy halide displacement).

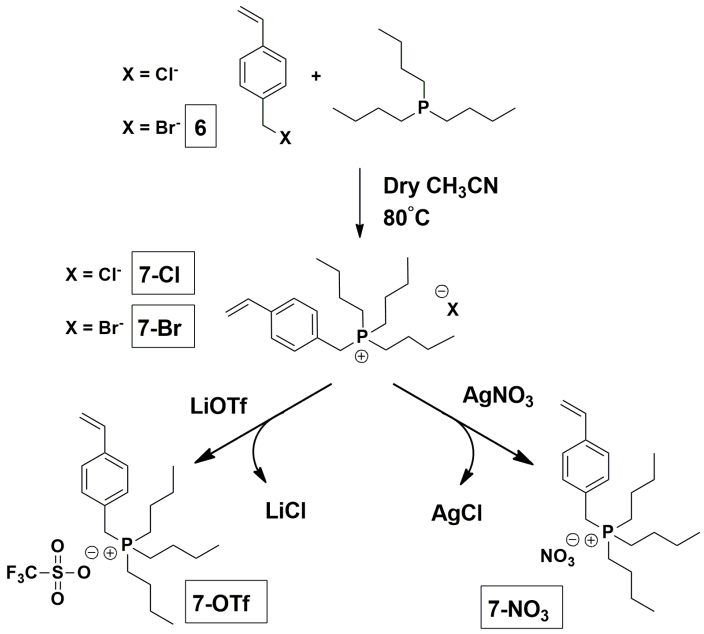

Scheme 1. Synthesis of phosphonium monomers

Compounds **7-NO_3** and **7-OTf** were produced through salt metathesis of the chloride monomer using $AgNO_3$ and LiOTf, respectively. In those cases, the removal of the chloride anion was confirmed through a precipitation test using lithium triflate or silver nitrate accordingly, where the absence of precipitate (AgCl or LiCl) was taken as complete Cl^- removal. The identity of the new salts was confirmed using ESI mass spectrometry in both positive and negative ion detection modes.

The relative degree of anion-cation interaction for the monomers in $CDCl_3$ was determined from the relative chemical shifts of the peaks corresponding to the benzylic methylene protons in the ^1H NMR spectra. As the extent of cation-anion interaction decreased going from the chloride to triflate counterion, the chemical shifts of those peaks decreased (Figure 2, Table 1). When salt **7-Cl** was exposed to solvents mixtures ranging from a low dielectric constant solvent (100% $CDCl_3$) to a higher one (100% CD_3OD), the chemical shift of the alpha methylene protons decreased with increasing solvent polarity (Figure 3). The decrease in chemical shifts may have been due to a greater interaction between the phosphonium and solvent dipoles as the anion moved away from the cation. These data show that there was little difference in the coordination between the chloride and bromide salts, whereas the nitrate association was much weaker than that of the halides and the triflate anion even less so in chloroform. While this trend does not follow what one would expect from electronegativity arguments, it is possible that the paramagnetic contributions from the phosphorus atom are dominant and impose on the chemical shifts observed for the cation-anion pairs. The trend may also arise from stronger cation-π interactions[26,27] between the phosphonium and the phenyl rings in the case of the more weakly coordinating anions.

	Benzylic Methylene δ	K_{ow}
7-Cl	4.28	0.41 ± 0.02
7-Br	4.26	0.64 ± 0.04
7-NO_3	3.93	1.34 ± 0.005
7-OTf	3.78	2.18 ± 0.27

Table 1. Chemical shift values of the benzylic methylene protons and the octanol-water partition coefficients of the monomer salts.

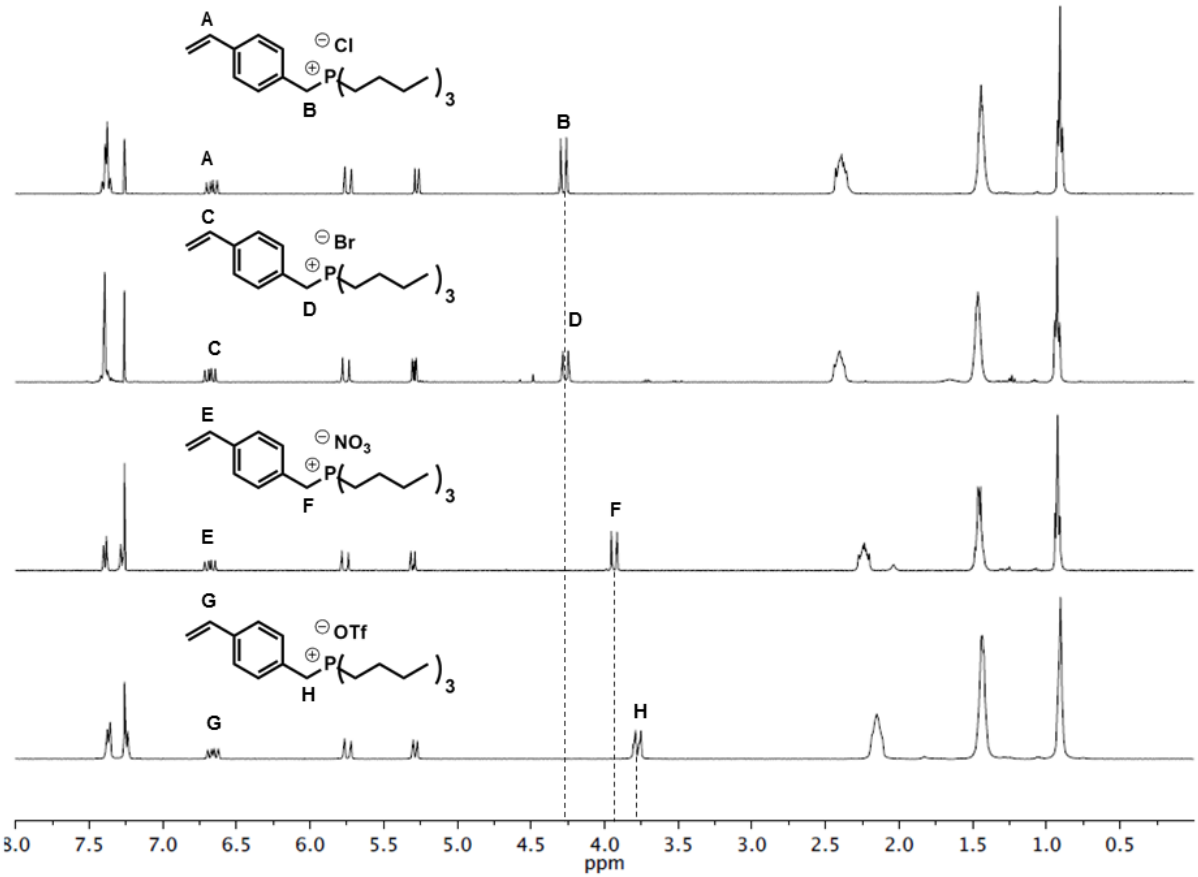

Figure 2. ^{1}H NMR spectra ($CDCl_3$, 400 MHz) of the phosphonium monomers indicating the change in chemical shift of the benzylic methylene protons with the change of the anion.

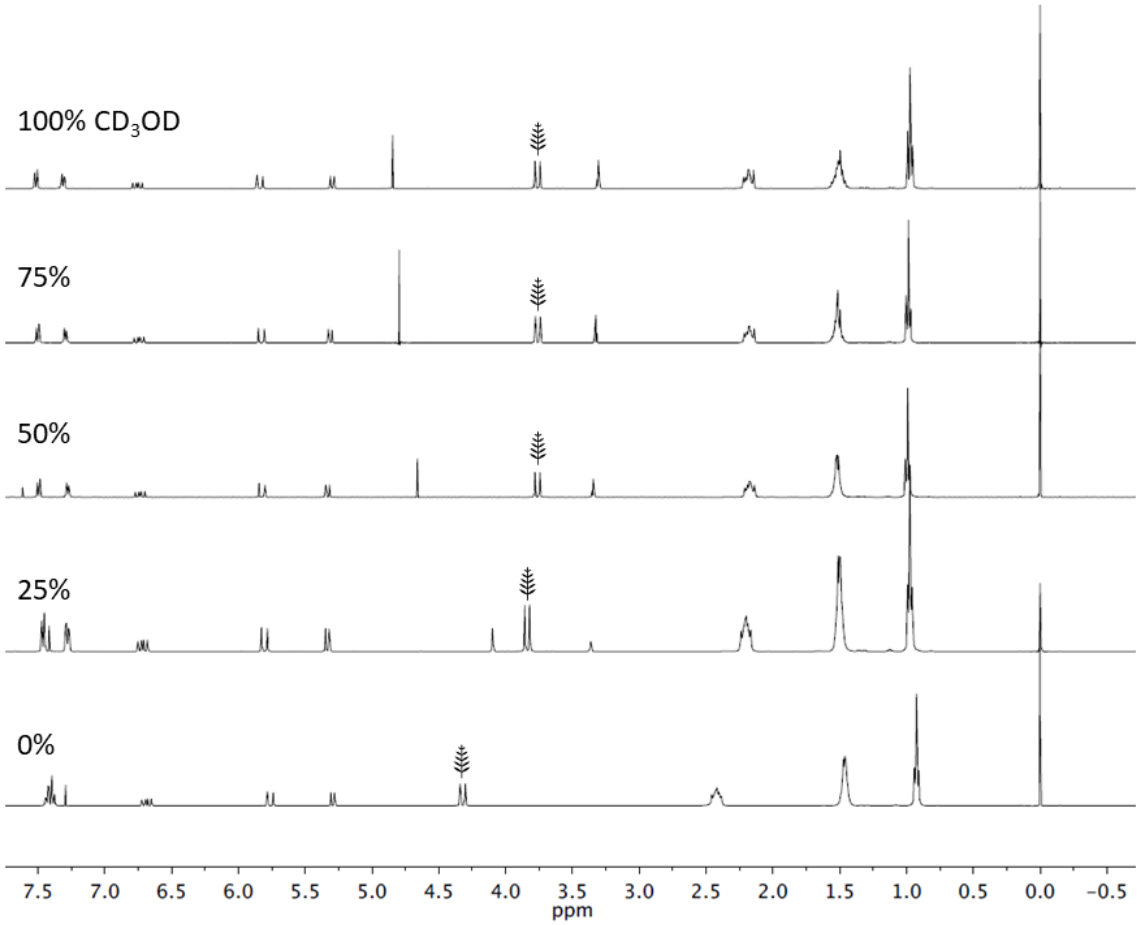

Figure 3. ^{1}H NMR solvent tritration of **7-Cl** in 100% CD_3OD to 0% CD_3OD (100% $CDCl_3$), referenced relative to Me_4Si. Branch symbol indicates the benzyl methylene proton signal.

Octanol/Water Partition Coefficient

The solubility behavior of the different **7-X** repeat units played a key role in the self-assembly of the BCPs by altering the energy of interaction between the hydrophilic phosphonium block and the water. We selected the octanol/water partition coefficient (K_{OW}) as an indicator of the monomer solubility and thus overall hydrophobicity. The presence of the phosphorus atom in the monomers provided a convenient handle for the spectroscopic determination of the amount of **7-X** in solution relative to an internal standard. This allowed the concentration of **7-X** to be measured in octanol after its partitioning between octanol and water. The K_{ow} values are listed in

Table 1. When the value K_{ow} is greater than 1, as in the case of **7-OTf** or **7-NO_3,** the compound is considered hydrophobic. Higher hydrophobicity should translate into an increased energy of interaction between the **P(PX)** block and water. This increased energy of interaction should lead to a smaller corona as the interaction between **P(PX)** chains should became more favorable than their interaction with the solvent. On the other hand, **7-Cl** and **7-Br** could be considered hydrophilic and should have had favorable interactions with water.

Synthesis of a Polystyrene MacroRAFT Agent

The morphological properties of nano-materials formed by the aqueous self-assembly of amphiphilic BCPs are sensitive to the volume fractions of the blocks. The volume fraction of each block depends on both the identity of the polymer and its DP. As the goal was to explore the effects of the different anions, the differences in the DP of the different **PS-*b*-P(PX)** polymers needed to be negligible. Self-assembly is also dependent on the *Đ* of the BCPs so it was important to achieve a similar, and ideally low *Đ,* for each copolymer. This was achieved by RAFT polymerization using a previously reported fluorinated RAFT agent (Scheme 2).[23] The fluorine groups provided a handle to assist in characterization of the block polymers as described in the supplementary information. The PS macroRAFT agent was synthesized first, which allowed for the absolute determination of M_n and M_W using SEC calibrated with polystyrene standards. A relatively high DP for the PS was desired, as the smallest monomer, **7-Cl**, has a 3.4-fold greater mass than that of styrene. The resulting polymer had a M_n of 39400 g/mol and a *Đ* of 1.17, which demonstrated good control over the polymerization. This corresponds to a DP_n of 390.

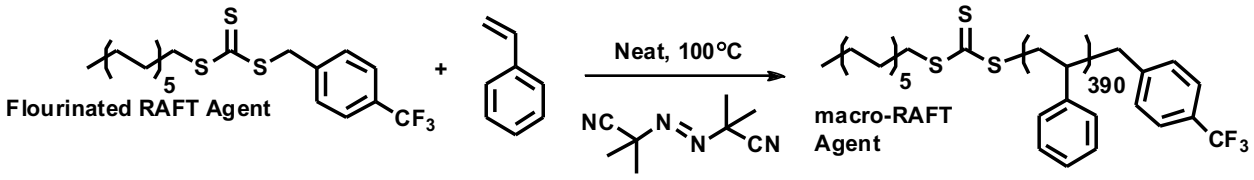

Scheme 2. Synthesis of polystyrene macro-RAFT agent.

Synthesis and Characterization of PS_{390}-*b*-P(PX)$_7$

The Eisenberg group has reported that relatively low volume fractions of the annealed polyelectrolyte polyacrylate (PAA) provided interesting and higher ordered morphologies of PS-*b*-PAA BCPs.[10] For this reason the **P(7X)** block was targeted at a short length of 7 repeat units. A length of 7 repeat units gives a hydrophilic mass fraction of approximately 6 - 9%, greater than those reported for the PS-*b*-PAA copolymers reported by Eisenberg. The **PS_{390}-b-P(7-X)$_7$** BCPs were prepared from the polystyrene macroRAFT agent, and an excess of the **7-X** monomer was used to avoid undesirable side reactions typically seen at high monomer conversions (Scheme 3).[28]

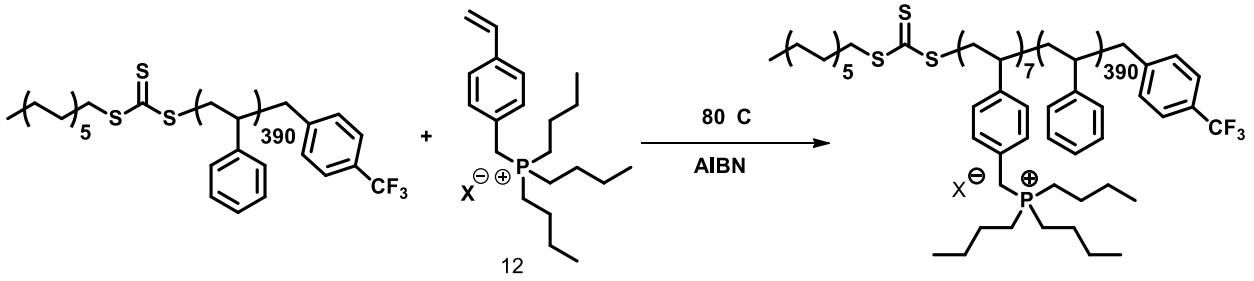

Scheme 3. Synthesis of **PS_{390}-b-P(7-X)$_7$**

The ability of the polystyrene macro-RAFT agent to control the polymerization of the **7-OTf** was monitored by ^{1}H NMR spectroscopy using a previously reported procedure.[29] Briefly, the disappearance of the vinylic protons indicated the consumption of monomer relative to the methyl protons on the phosphonium. A linear relationship between the natural logarithm of the

monomer conversion and time was observed indicating that the RAFT agent provided good control over the polymerization (Figure 4).

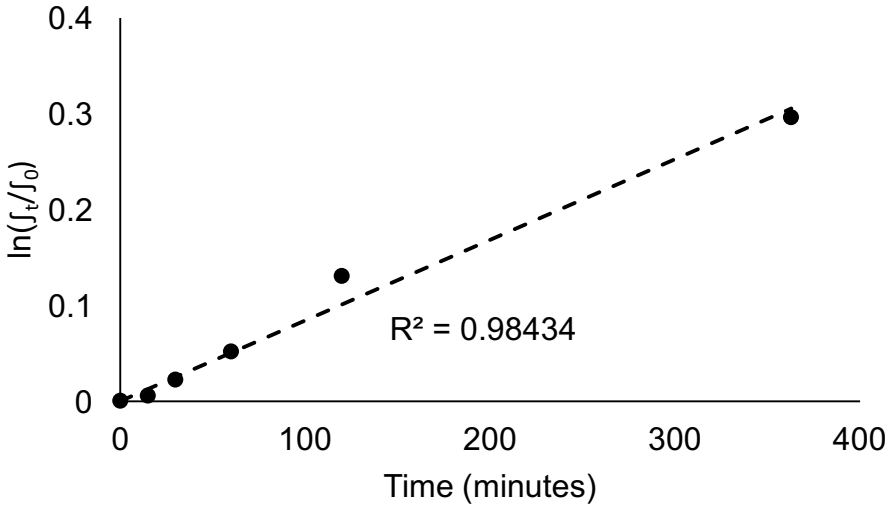

Figure 4. Pseudo- 1st order kinetics of the polymerization **7-OTf** by **PS** MacroRAFT where $\int_t$ is the integration of an alkene signal in the ^{1}H NMR spectrum of an aliquot of the reaction mixture and $\int_0$ is the initial integration of that same peak, relative to the integration of the phosphonium methyl groups, the chemical shift of which is unaltered between monomer and polymer.

Having demonstrated control over the polymerization, chain extension from the PS MacroRAFT agent with monomer **7-OTf** to afford the desired block copolymer was performed first because this monomer has two separate NMR spectroscopic handles available to determine the DP of the phosphonium block. The trifluoromethyl group on the RAFT agent combined with the trifluoromethyl group on the anion allow for end-group analysis of the **PS$_{390}$-*b*-P(7-OTf)$_7$** copolymer by ^{19}F NMR spectroscopy. In addition, the known DP of the PS block can be used to determine the DP of the **P(7-OTf)** block by comparing the relative integrations of the methyl protons from the phosphonium block with the total integration of all other alkyl protons (Figure S11). Both methods provided consistent DP$_n$ values, demonstrating the reliability of the ^{1}H NMR

spectroscopic method for the other copolymers, where the ^{19}F method could not be applied. It was confirmed that each of the product BCPs had a DP_n of 7 for the phosphonium block. The SEC traces of the BCPs also confirmed that low *Đ* values were maintained (Table 2), however due to the nature of the standard used for the salt SEC system the M_n reported is from ^1H NMR spectroscopic data, which was more reliable. Thermal characterization of the polymers showed that the presence of the phosphonium generally resulted in an increased decomposition temperature, in all cases except for **PS_{390}-*b*-P(7-NO_3)$_7$**. No T_g for the phosphonium blocks was observed in the thermograms (Figures S15-S19) likely due to the relatively low mass fraction of the phosphonium blocks in the polymers.

Polymer	M_n (kg/mol)	Decomposition Onset Point (°C)	T_g (°C)	*Đ*	CAC (μg/mL)
MacroRAFT	39.4[a]	300	103	1.1	N/A
PS_{390}-*b*-P(7-Cl)$_7$	41.9	332	101	1.4	39
PS_{390}-*b*-P(7-Br)$_7$	42.2	333	104	N/A	21
PS_{390}-*b*-P(7-OTf)$_7$	42.7	338	105	1.4	28
PS_{390}-*b*-P(7-NO_3)$_7$	42.1	304	98	1.4	24

Table 2. Polymer characterization. [a]M_n determined by SEC; all others determined by ^1H NMR spectroscopy.

Preparation and Characterization of Self-Assembled Particles

Aqueous nanoprecipitation of the BCPs was performed to investigate the effect the anions had on the aqueous self-assembly of the BCPs. DMF and THF were used not only for their ability to fully dissolve the polymer chains, but they provided differences in polarity while retaining water miscibility at any solvent ratio. DMF has a smaller polarity difference with water than THF does, and so the PS block was expected to precipitate at lower solvent:water ratios in the DMF:water

system than in the THF:water systems. Additionally, two different rates of water addition were investigated to assess for differences in kinetic and thermodynamic control of assembly formation. The rapid switch from organic to aqueous environment involved the addition of organic solvent into water, ensuring that there was always an excess of water. That induced the BCPs to adopt kinetically trapped morphologies as the polystyrene core forming block remained insoluble throughout particle formation. The slow addition system involved slow water addition over ten minutes to allow the polymers to adopt a thermodynamically favorable morphology as the water content slowly increased and the PS remained solvated by the organic solvent before becoming trapped into a final morphology. Further solvent annealing for some samples also enabled the glassy PS core to remain partially solvated allowing for thermodynamic equilibrium to be reached for the morphologies. The dodecyl chain at the end of the phosphonium block was not removed prior to self-assembly as the chain is flexible enough to fold into the hydrophobic pocket created by the polyphosphonium backbone. TEM analysis of particles formed from BCP with the terminal RAFT group removed did not show a difference in morphological properties (see Figure S23).

The effect of the anion on the aqueous self-assembly was explored by measuring the size distributions of the particles that formed during nanoprecipitation. The diameter distributions were measured by DLS. Table 3 lists the mean z-average diameters and polydispersity indices (PDIs) of the different systems determined by the cumulants analysis of the raw DLS data. The nanoprecipitation performed with slow addition of water resulted in the largest particles, as the particles had more time to reach thermodynamic equilibrium. As the water content was slowly increased, the polymers remained dissolved and the core-forming PS block remained partially solvated, allowing the assemblies to grow larger. Comparing the z-average diameters produced

from the different organic solvents also revealed that the particles produced by the DMF system were systematically smaller than the particles produced by the same polymers from the THF systems (Table 3). This was likely due to the smaller difference in polarity between water and DMF, which induced kinetic trapping to occur earlier in the process. The low variability (the highest is **PS_{390}-*b*-P(P-OTf)$_7$** with a standard deviation of 28%) for most of the samples showed that the nanoprecipitation method was highly reproducible for the kinetically trapped particles in terms of the resulting particle size distributions. The low mean PDI values for the samples also indicated that the particles had narrow size distributions, as measured by DLS.

	DMF				THF			
	Kinetic Trapping		Solvent Annealed		Kinetic Trapping		Solvent Annealed	
Counter anion	Slow H_2O addition	Fast addition to H_2O	Slow H_2O addition	Fast addition to H_2O	Slow H_2O addition	Fast addition to H_2O	Slow H_2O addition	Fast addition to H_2O
Chloride	77 ± 1 (0.16 ± 0.01)	58 ± 3 (0.25 ± 0.03)	169 ± 31 (0.10 ± 0.04)	60 ± 1 (0.18 ± 0.01)	176 ± 2 (0.27 ± 0.16)	55 ± 1 (0.17 ± 0.02)	503 ± 74 (0.23 ± 0.05)	56 ± 7 (0.17 ± 0.06)
Bromide	67 ± 2 (0.19 ± 0.01)	24 ± 1 * (0.13 ± 0.02)	177 ± 21 (0.20 ± 0.04)	27 ± 2 (0.19 ± 0.01)	163 ± 8 (0.06 ± 0.02)	39 ± 4 (0.27 ± 0.05)	406 ± 29 (0.11 ± 0.03)	37 ± 1 (0.25 ± 0.02)
Nitrate	78 ± 3 (0.21 ± 0.03)	24 ± 1 * (0.13 ± 0.01)	154 ± 44 (0.14 ± 0.02)	26 ± 1 (0.18 ± 0.03)	217 ± 3 (0.29 ± 0.21)	38 ± 2 (0.31 ± 0.02)	275 ± 32 (0.11 0.06)	33 ± 2 (0.22 ± 0.03)
Triflate	84 ± 4 (0.19 ± 0.02)	23 ± 1 (0.35 ± 0.06)	184 ± 12 (0.22 ± 0.08)	42 ± 1 (0.16 ± 0.02)	137 ± 2 (0.13 ± 0.03)	49 ± 5 (0.28 ± 0.04)	225 ± 3 (0.06 ± 0.02)	30 ± 1 (0.26 ± 0.03)

Table 3. Mean z-average values and PDI values (indicated in brackets) measured by DLS for the different solvent systems and addition rates. *Samples filtered through 0.22 μm filters.

The method of assembly influenced the size distributions of the particles formed (Table 3). In all different methods of assembly with the exception of the solvent annealed particles prepared by slow addition of water into the DMF BCP solution, the particle sizes obtained with the different anions were statistically different from one another (Table S1). Particles formed from **PS_{390}-*b*-P(7-Cl)$_7$** were consistently larger than those formed from **PS_{390}-*b*-P(7-Br)$_7$** ($p < 0.05$, Table S2). Given the relatively similar K_{ow} of the chloride and bromide monomers ($K_{ow,[7]Cl} = 0.41$, $K_{ow,[7]Br} = 0.64$) and the relatively similar anion-cation interaction evidenced by the similar chemical shifts (Figure 2), the most relevant difference between the systems was the size of the anion. As Br^- is larger than Cl^-, the relative hydrophilic volume was expected to increase, requiring a greater curvature to pack into the self-assembled particles, thereby favoring smaller particle diameters. The same trend was also observed between **PS_{390}-*b*-P(7-Cl)$_7$** and the remaining BCPs except for the kinetically trapped particles formed by the fast addition water into a THF solution of the BCPs where the particles formed by **PS_{390}-*b*-P(7-NO_3)$_7$** were larger than those formed by **PS_{390}-*b*-P(7-Cl)$_7$**. This result suggests that overall the size of the anion played an important role in the formation of the particles.

Comparing the particle diameters of **PS_{390}-*b*-P(7-Br)$_7$** assemblies with those formed by **PS_{390}-*b*-P(7-NO_3)$_7$**, the only instances when the distributions were statistically different were when the particles were formed by slow addition of water into the BCP solution (Table S2). Given the similar sizes of these two anions[25] the difference in particle size likely arose from their different K_{ow} values. In the particles formed by kinetic trapping, those formed by the **PS_{390}-*b*-P(7-Br)$_7$** BCP were smaller than those formed by **PS_{390}-*b*-P(7-NO_3)$_7$**. This can be explained by

the higher hydrophilicity of the Br^- anion, which would increase the relative hydrophilic volume fraction of the BCP and result in a higher curvature to favour smaller particles.

In the case of particles formed from DMF BCP solutions, **PS_{390}-*b*-P(7-Br)$_7$** formed significantly smaller particles than **PS_{390}-*b*-P(7-OTf)$_7$** (Table S2). The opposite was true for the THF systems of these block copolymers, except for the kinetically trapped particles formed by fast addition of water. The lack of consistent trends may result from differences in both the sizes and the hydrophilicities of these two anions. The data do not lend themselves to readily discernable patterns.

Particles formed from **PS_{390}-*b*-P(7-NO_3)$_7$** were significantly smaller than those formed from **PS_{390}-*b*-P(7-OTf)$_7$** when they were prepared kinetically. This is consistent with the higher hydrophilicity of NO_3^-, which would increase the relative hydrophilic block fraction for **PS_{390}-*b*-P(7-NO_3)$_7$** relative to **PS_{390}-*b*-P(7-OTf)$_7$**, leading to higher curvature and consequently smaller assemblies. On the other hand, NO_3^- is smaller than TfO^-, which would be expected to result in larger assemblies due to a decrease in hydrophilic volume fraction, and this was indeed observed when the assemblies were prepared by kinetic trapping following slow addition of water into a THF solution of the BCPs.

Particles formed by the fast addition of both THF and DMF BCP solutions into H_2O, followed by kinetic trapping, had very similar diameters for **PS_{390}-*b*-P(7-Br)$_7$**, **PS_{390}-*b*-P(7-NO_3)$_7$** and **PS_{390}-*b*-P(7-OTf)$_7$**. The fast addition of organic solvent to water with kinetic trapping was expected to result in the most rapid formation of the particles from the fully dissolved polymer chains, as at all points in the mixing of the solvent there was a large excess of water in the system. This shows that the effect of the anion was less important when the particles were formed by kinetic trapping. However, the solvent annealed particles had greater variabilities in

diameter. This is likely due to the greater role the anion played when the particles were allowed to reach a more thermodynamically stable state.

The particle sizes and morphologies were also investigated in the dried state using TEM imaging. Previous work on the self-assembly of low polycation content BCPs revealed the formation of higher-order morphologies such as vesicles or lamellae.[12] However, the present work shows that despite a very low hydrophilic content, the dominant morphologies are micelles and larger solid nanoparticles (NP) (Table 4), Figure 5). Micellar morphologies as seen in Figure 5b, were present in most of the self-assembled suspensions (Table 4). When particles were allowed more time to reach equilibrium during formation, the presence of larger solid nanoparticles developed (Figure 5c-e). In some cases, very large particles were present, such as for the slow addition of water into a THF solution of **PS_{390}-*b*-P(7-NO_3)$_7$** as shown in Figure 5C. In those cases there was a clear distinction between the outer region and the inner region of the particles based on their differences in electron density. These particles have been assigned as solid nanoparticles, since they are too large to be true micelles. Interestingly they exhibit a distinct difference in electron density between the inner and outer regions of the particles. Attempts to determine the composition of the outer region of the particles were unsuccessful.

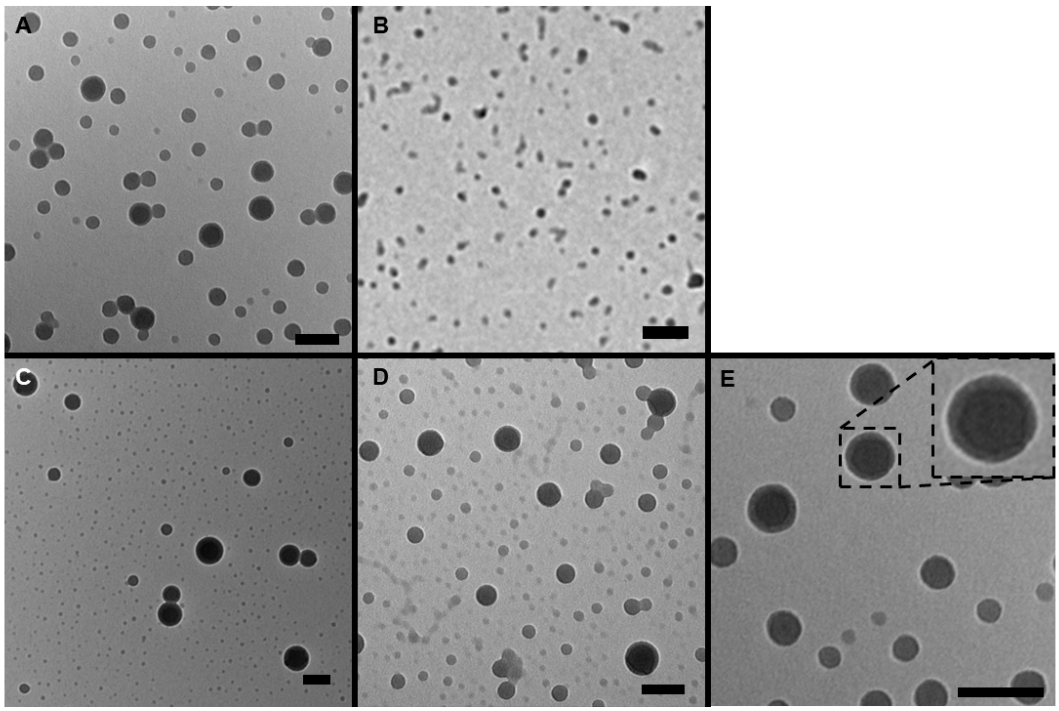

Figure 5. TEM images of A) **PS_{390}-*b*-P(7-Cl)$_7$** particles formed by slow addition of water into DMF; B) **PS_{390}-*b*-P(7-Br)$_7$** particles formed by fast addition of water into DMF; C) **PS_{390}-*b*-P(7-NO_3)$_7$** particles formed by slow addition of water into THF; D) **PS_{390}-*b*-P(7-OTf)$_7$** particles formed by fast addition of water into THF E) Zoom of 5A to show contrast difference on particles along with expanded view of one of the particle. Scale bars are 100 nm.

	DMF				THF			
	Kinetic Trapping		Solvent Annealed		Kinetic Trapping		Solvent Annealed	
Counter anion	Slow H_2O addition	Fast addition to H_2O	Slow H_2O addition	Fast addition to H_2O	Slow H_2O addition	Fast addition to H_2O	Slow H_2O addition	Fast addition to H_2O
Chloride	M	M	M, NP	M	M, NP	M, NP	M, NP	M
Bromide	M	M	M, NP	M	M, NP	M	M, NP	M
Triflate	M	M	M, NP	M	M, NP	M, NP	M, NP	M
Nitrate	M, NP	M	M, NP	M	M, NP	M	M, NP	M

Table 4. Morphology of particles formed by nanoprecipiation as determined by TEM; M = micelles, NP = solid nanoparticles.

The TEM image analysis showed that the diameter distribution of the particles for the fast addition of non-selective solvent into the water agreed best with those determined from DLS (Figure S24). In general, the diameters measured by TEM were smaller than those measured by DLS. This may arise from two key factors: (i) In the solution phase the hydrophilic blocks were hydrated and in extended conformations, whereas in the dry state they collapsed; (ii) in DLS measurements the larger particles scatter light more effectively (scattered light intensity $\propto r^6$), which tends to emphasize a small population of larger particles, thereby increasing the z-average diameter. On the other hand, analysis of TEM images provides a number-based distribution. This is illustrated well in Figure 5C where there are two distinct distributions of particles from the slow addition of water into a THF solution of $\mathbf{PS_{390}}$-***b***-$\mathbf{P(7\text{-}NO_3)_7}$. As such, the diameters obtained from the TEM image analyses are smaller than those obtained from DLS, and in some cases the relative orders of mean sizes are also different for the different systems. Most importantly however is that there was no apparent effect of the anion identity on the morphology of the particles. As stated earlier, the expectation was that by varying the anion identity, the changes in hydrophilicity and anion size would result in changes in the particle morphology This was not observed (Table 4). Instead, changes in particle size rather than morphology was the dominant effect.

Summary and Conclusions

This study explored the physical properties of several phosphonium monomers and their relationship to the morphological properties of nano-materials assembled from their copolymers. The monomer salts displayed an interesting relationship in that the degree of interaction between the charges in lipophilic solution provided a good prediction of the K_{ow} values for the salts. The

ability to make low *Đ* BCPs from the phosphonium monomer salts and their aqueous self-assembly from dilute solutions in THF and DMF was explored and their self-assembly led to nanoparticles with diameters ranging from 30 nm to > 200 nm, based on DLS and TEM analysis. The anions had reproducible effects on the sizes but not the morphologies of the nanoparticles. The differences between the particle diameters of the **PS_{390}-*b*-P(7-Cl)$_7$** and the other anion systems showed that anions of small size resulted in larger particles. In contrast, the relationships between the diameters of assemblies formed from **PS_{390}-*b*-P(7-Br)$_7$**, **PS_{390}-*b*-P(7-NO_3)$_7$**, and **PS_{390}-*b*-P(7-OTf)$_7$** were more complex, arising from different and sometimes competing effects of anion size and hydrophilicity. This work is important in providing new insights into the effects of counterions on self-assembly of polyelectrolytes. Future work exploring the relationship may consider varying only the anion-cation interaction, or the hydrophilicity of similar sized anions in order to obtain a clearer picture of the relationship between anion identity and assembly size and morphology.

Associated Content

Multinuclear NMR, ATR-IR spectra, TEM images, DSC and TGA plots and GPC data as well as a guide to interpretation of box and whisker plots are provided in the supporting information section available free of charge on the ACS Publications website at DOI:

Acknowledgements

The authors thank the Natural Science and Engineering Council of Canada, Canada foundation for Innovation, Cytec-Solvay Group and the University of Western Ontario for financial support.

References

(1) Chen, G.; Roy, I.; Yang, C.; Prasad, P. N. Nanochemistry and Nanomedicine for Nanoparticle-based Diagnostics and Therapy. *Chem. Rev.* **2016**, *116*, 2826–2885.
(2) Mura, S.; Nicolas, J.; Couvreur, P. Stimuli-responsive Nanocarriers for Drug Delivery. *Nat. Mater.* **2013**, *12*, 991–1003.
(3) Kamaly, N.; Yameen, B.; Wu, J.; Farokhzad, O. Degradable controlled-release Polymers and Polymeric Nanoparticles: Mechanisms of Controlling Drug Release. *Chem. Rev.* **2016**, *116*, 2602-2663
(4) Duncan, R. The Dawning Era of Polymer Therapeutics. *Nat. Rev. Drug Discov.* **2003**, *2*, 347–360.
(5) Elsabahy, M.; Heo, G. S.; Lim, S.; Sun, G.; Wooley, K. L. Polymeric Nanostsructures for Imaging and Therapy. *Chem. Rev.* **2015**, *115*, 10967–11011.
(6) Chinen, A. B.; Guan, C. M.; Ferrer, J. R.; Barnaby, S. N.; Merkel, T. J.; Mirkin, C. A. Nanoparticle Probes for the Detection of Cancer Biomarkers, Cells, and Tissues by Fluorescence. *Chem. Rev.* **2015**, *115*, 10530–10574.
(7) Lu, J.; Dimroth, J.; Weck, M. Compartmentalization of Incompatible Catalytic Transformations for Tandem *J. Am. Chem. Soc.* **2015**, *137*, 12984-12989
(8) Lee, L. C.; Lu, J.; Weck, M.; Jones, C. W. Acid-Base Bifunctional Shell Cross-linked Micelle Nanoreactor for One-Pot Tandem Reaction. *ACS Catal.* **2016**, *6*, 784–787.
(9) Lu, J.; Liang, L.; Weck, M. Micelle-based Nanoreactors Containing Ru-porphyrin for the Epoxidation of Terminal Olefins in Water *J. Mol. Catal. A Chem.* **2016**, *417*, 122–125.
(10) Mai, Y.; Eisenberg, A. Self-assembly of Block Copolymers. *Chem. Soc. Rev.* **2012**, *41*, 5969–5985.
(11) Cameron, N. S.; Corbierre, M. K.; Eisenberg, A. 1998 E.W.R. Steacie Award Lecture Asymmetric Amphiphilic Block Copolymers in Solution: a Morphological Wonderland *Can. J. Chem.* **1999**, *77*, 1311–1326.
(12) Discher, D. E.; Eisenberg, A. Polymer Vesicles. *Science.* **2002**, *5583*, 967-973.
(13) Nigmatullin, R.; Gao, F. Onium-functionalised Polymers in the Design of Non-leaching Antimicrobial Surfaces. *Macromol. Mater. Eng.* **2012**, *297*, 1038–1074.
(14) Carmona-Ribeiro, A. M.; de Melo Carrasco, L. D. Cationic Antimicrobial Polymers and Their Assemblies. *Int. J. Mol. Sci*. **2013**, 14, 9906–9946.
(15) Aboudzadeh, M. A.; Muñoz, M. E.; Santamaría, A.; Marcilla, R.; Mecerreyes, D. Facile Synthesis of Supramolecular Ionic Polymers that Combine Unique Rheological, Ionic Conductivity, and Self-healing Properties. *Macromol. Rapid Commun.* **2012**, *33*, 314–318.
(16) Eisenberg, A.; Kim, J. *Introduction to Ionomers*; John Wiley & Sons, Inc.: New York, 1998.
(17) Borisov, O. V.; Zhulina, E. B. Effect of Salt on Self-assembly in Charged Block Copolymer Micelles. *Macromolecules* **2002**, *35*, 4472–4480.
(18) Solomatin, S. V.; Bronich, T. K.; Bargar, T. W.; Eisenberg, A.; Kabanov, V.; Kabanov, A. Environmentally Responsive Nanoparticles from Block Ionomer Complexes: Effects of pH and Ionic Strength. *Langmuir* **2003**, *19*, 8069–8076.
(19) Solomatin, S. V.; Bronich, T. K.; Eisenberg, A.; Kabanov, V.; Kabanov, A. Colloidal Stability of Aqueous Dispersions of Block Ionomer Complexes: Effects of Temperature and Salt. *Langmuir* **2004**, *20*, 2066–2068.

(20) Förster, S.; Hermsdorf, N.; Leube, W.; Schnablegger, H.; Regenbrecht, M.; Akari, S.; Lindner, P.; Böttcher, C. Fusion of Charged Block Copolymer Micelles into Toroid Networks. *J. Phys. Chem. B* **1999**, *103*, 6657–6668.
(21) Guo, J.; Zhou, Y.; Qiu, L.; Yuan, C.; Yan, F. Antibacterial Vesicles by Direct Dissolution of a Block Copolymer in Water. *Polym. Chem.* **2013**, *4*, 255-259
(22) Vijayakrishna, K.; Mecerreyes, D.; Gnanou, Y.; Taton, D. Polymeric Vesicles and Micelles Obtained by Self-assembly of Ionic Liquid-based Block Copolymers Triggered by Anion of Solvent Exchange. *Macromolecules* **2009**, *42*, 5167–5174.
(23) Hadadpour, M.; Gwyther, J.; Manners, I.; Ragogna, P. J. Multifunctional Block Copolymer: Where Polymetallic and Polyelectrolyte Blocks Meet. *Chem. Mater.* **2015**, *27*, 3430–3440.
(24) Tindale, J. J.; Hartlen, K. D.; Alizadeh, A.; Workentin, M. S.; Ragogna, P. J. Maleimide-modified Phosphonium Ionic Liquids: a Template Towards (multi)task-specific Ionic Liquids *Chem. Eur. J.* **2010**, *16*, 9068–9075.
(25) Masterton, W. L.; Bolocofsky, D.; Lee, T. P. Ionic Radii From Scaled Particle Theory of the Salt Effect. *J. Phys. Chem.* **1971**, *75*, 2809–2815.
(26) Dougherty, D. A. Cation-π interactions in chemistry and biology: a new view of benzene, phe, tyr, and trp. *Science* **1996**, *271*, 163 - 168
(27) Kearney, P. C.; Mizoue, L. S.; Kumpf, R. A.; Forman, J. E.; McCurdy, A.; Dougherty, D. A. Molecular recognition in aqueous media. New binding studies provide further insights into the cation-π interaction and related phenomena *J. Am. Chem. Soc.* **1993**, *115*, 9907 - 9919
(28) Moad, G.; Rizzardo, E.; Thang, S. H. Radical Addition-fragmentation Chemistry in Polymer Synthesis. *Polymer* **2008**, *49*, 1079-1131
(29) Cuthbert, T. J.; Harrison, T. D.; Ragogna, P. J.; Gillies, E. R. Synthesis, Properties, and Antibacterial Activity of Polyphosphonium Semi-interpenetrating Networks. *J. Mater. Chem. B* **2016**, *4*, 4872–4883.